Macromolecules

pubs.acs.org/Macromolecules Article

Bottlebrushes and Combs with Bimodal Distribution of the Side Chains: Diagram of States and Scattering Function

Haley Starvaggi, Yuan Tian, Heyi Liang, and Andrey V. Dobrynin*

Cite This: *Macromolecules* 2021, 54, 1818–1828 Read Online

ACCESS | Metrics & More | Article Recommendations

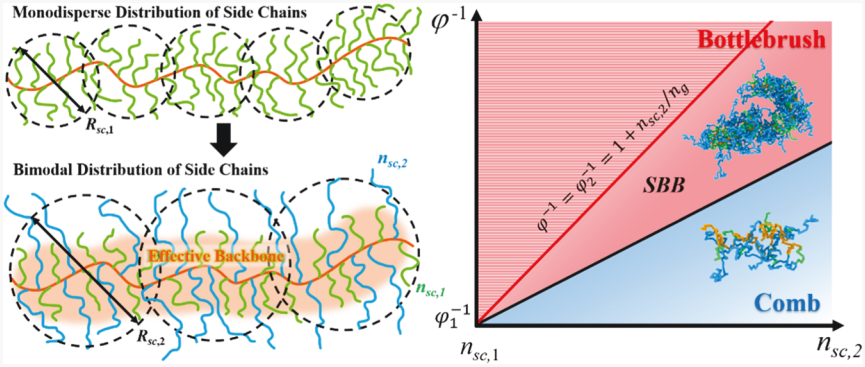

ABSTRACT: We use a combination of scaling analysis, random phase approximation (RPA) calculations, and coarse-grained molecular dynamics (MD) simulations to elucidate properties of graft polymers with a bimodal distribution of side chains in a melt. In our scaling analysis, a two-step approach is used to classify graft polymers with the grafting density of side chains $1/n_g$, fraction of short side chains f, and degree of polymerization (DP) of short DP = $n_{sc,1}$ and long DP = $n_{sc,2}$ side chains into combs and bottlebrushes. First, a diagram of states of the monodisperse graft polymers with short side chains of DP = $n_{sc,1}$ and grafting density $1/n_g$ is constructed. During the second step, these graft polymers are considered as backbones with the effective Kuhn length to which the longer side chains are attached at grafting density $(1 - f)/n_g$. This approach allows the reduction of four-dimensional architectural parameter space (n_g, $n_{sc,1}$, $n_{sc,2}$, f) into two two-dimensional projections. In the framework of this representation, we extended the concept of crowding parameter Φ, describing the degree of mutual interpenetration of the side chains belonging to neighboring macromolecules, and applied it to derive the effective Kuhn length of graft polymers with two types of side chains as a function of Φ. The predictions of the scaling model for the effective Kuhn length and diagram of states are confirmed by coarse-grained MD simulations. The evolution of the peak position in the static structure factor $S(q)$ obtained in these simulations is analyzed by using the expression for $S(q)$ derived in the framework of RPA. In the bottlebrush regime, the peak position in the scattering function is shown to scale as $q^* \sim \langle n_{sc} \rangle^{-0.39 \pm 0.02}$ with the number average DP of the side chains $\langle n_{sc} \rangle$, which is in good agreement with the result of the RPA calculations, $q^* \sim \langle n_{sc} \rangle^{-3/8}$. However, this is a weaker dependence than one expected for q^* to be associated with the inter-backbone distance $q^* \sim \langle n_{sc} \rangle^{-0.5}$.

INTRODUCTION

Graft polymers (combs or bottlebrushes) are made by grafting polymer chains (side chains) to linear chain backbones.[1−6] The unique physical properties of this class of polymers are directly controlled during the synthesis stage by changing the degree of polymerization (DP) of the side chains, n_{sc}, and their grafting density, $1/n_g$. Side chains play a dual role by "diluting" and at the same time stiffening the backbones. This dual nature of the side chains is manifested in the suppression of the entanglements,[7−16] opening a path toward design and synthesis of solvent-free supersoft elastomers with mechanical properties mimicking those of biological tissue.[14,17−23]

Current understanding of the effect of the side chains on conformations of graft polymers and their classification into combs and bottlebrushes is based on the concept of the crowding parameter, Φ, quantifying the degree of interpenetration between side chains and backbones of neighboring macromolecules.[11,24,25] Graft polymers for which crowding parameter $\Phi < 1$ are called combs, while systems of macromolecules with $\Phi > 1$ are referred to as bottlebrushes.

Received: November 22, 2020
Revised: January 12, 2021
Published: February 8, 2021

https://dx.doi.org/10.1021/acs.macromol.0c02610
Macromolecules 2021, 54, 1818−1828

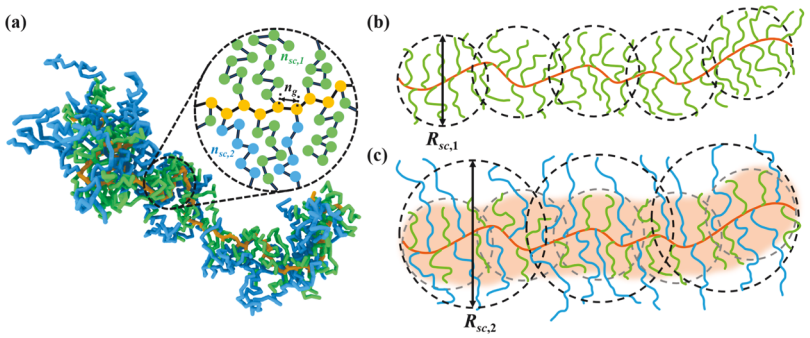

Figure 1. (a) Graft polymer with two different types of side chains. Backbone monomers are shown in orange; monomers belonging to short and long side chains are colored in green and blue, respectively. (b,c) Schematic representation of different blob structure used to describe conformations of graft polymers with bimodal side chains.

In combs, the side chains dilute the backbone keeping macromolecular conformations close to those of linear polymers. In the case of bottlebrushes, the steric repulsion between side chains results in backbone stiffening. Specifically, it was shown in the framework of the scaling approach and by coarse-grained molecular dynamics (MD) simulations that in a melt, the bottlebrush Kuhn length is proportional to the crowding parameter.[24,25] This relationship between crowding parameter and Kuhn length was used to explain the effect of the graft polymer architecture on entanglement plateau modulus in the comb and bottlebrush regimes[11,13,14] and was implemented in design principles of solvent-free elastomer made of graft polymer strands.[14,19,21−23] Furthermore, backbone stiffening and dilution by side chains were used to explain self-assembly in copolymers containing linear and graft polymer blocks and graft polymer blocks alone.[26−30]

However, despite the success in using graft polymers with a single type of side chains in the design of the solvent-free elastomers, the range of achievable variations in the system's mechanical properties is limited.[19,30,31] Therefore, to broaden the range of accessible parameters, we consider graft polymers with bimodal side chain distribution in a melt. This adds a degree of complexity in correlating system physical properties with molecular architecture and at the same time relaxes restrictions of macromolecular synthesis. To address complexity issues, we use a combination of the scaling analysis and coarse-grained MD simulations to describe the properties of this type of graft polymer. We begin with redefining the concept of the crowding parameter and use it in the construction of a diagram of states as a function of the molecular architecture and in the calculations of the effective Kuhn length. Then, to make a connection to experiments we calculate the scattering function and correlate its peak position with the macromolecular structure and properties.

SCALING MODEL OF GRAFT POLYMERS WITH BIMODAL DISTRIBUTION OF THE SIDE CHAINS

We begin with an analysis of different conformation regimes of graft polymers with the DP of the backbone N_{bb} and two different types of side chains as illustrated in Figure 1a. Side chains with DPs $n_{sc,1}$ and $n_{sc,2}$ are randomly attached to monomers of the backbone separated by n_g bonds between two neighboring grafting points. The shorter side chains have DP $n_{sc,1}$, while longer side chains consist of $n_{sc,2}$ monomers. The number fraction of the shorter side chains is equal to f resulting in the average number of the backbone bonds between short and long side chains to be equal to $n_{g,1} = n_g/f$ and $n_{g,2} = n_g/(1 - f)$, respectively. The backbones and side chains are made of identical monomers with the bond projection length l, Kuhn length b, and excluded volume v.

Complexity of the graft polymer chemical structure described by four structural parameters ($n_{sc,1}$, $n_{sc,2}$, n_g, f) requires a four-dimensional parameter space to classify different conformational regimes of this type of graft polymers. To overcome this complexity and simplify the analysis of the different regimes, we use a two-step approach in the classification of graft polymers with a bimodal distribution of the side chains. This reduces a four-dimensional parameter state to two two-dimensional projections. In particular, we first construct a diagram of states of the monodisperse graft polymers ($f = 1$) with short side chains of DP = $n_{sc,1}$ and grafting density $1/n_g$ (Figure 1b). During the second step, these graft polymers are considered as backbones with effective Kuhn length to which longer side chains are attached (Figure 1c). The steric interactions between longer side chains make the graft polymers even stiffer, increasing their effective Kuhn length and changing their conformations. The results from the renormalization of the backbone Kuhn length by the shorter and longer side chains are then used to calculate the diagram of states of graft polymers with bimodal side-chain distribution in terms of the effective Kuhn length of the monodisperse graft polymers with short side chains, DP of the long side chains, and graft polymer composition.

Diagram of States of Monodisperse Graft Polymers ($f = 1$). In our analysis of the different conformational regimes of graft polymers, we apply the concept of crowding parameter describing the degree of mutual interpenetration between different macromolecules in a melt developed in refs 24 and 25. Here, we consider the case of flexible side chains with the DP $n_{sc,1} \geq b/l$. The degree of interpenetration between graft polymers is quantified by calculating the volume fraction of monomers of a test macromolecule within its pervaded volume. Consider a test macromolecule as a chain of blobs of size equal to that of the side chains $D \approx R_{sc,1}$ with the number of monomers $g \approx n_{sc,1}$ (see Figure 1b). At low grafting density, both the side chains and backbones display statistics of a random walk. A crowding parameter, Φ_1, is defined as volume fraction of the monomers V_m belonging to the test macromolecule within the blob pervaded volume

$$\Phi_1 \equiv V_m/D^3 \approx g\varphi_1^{-1}\cdot v/D^3 \approx v(lb)^{-3/2}\varphi_1^{-1}n_{sc,1}^{-1/2} \quad (1)$$

where we introduced composition parameter

$$\varphi_1 = (1 + n_{sc,1}/n_g)^{-1} \quad (2)$$

https://dx.doi.org/10.1021/acs.macromol.0c02610
Macromolecules 2021, 54, 1818−1828

describing partitioning of monomers between a side chain and backbone spacer between two neighboring side chains. (Note that this definition of the crowding parameter is only correct for side chains longer than the spacers between them, $n_{sc,1} > n_g$. If the opposite inequality holds, $n_{sc,1} < n_g$, the blobs are spacers between side chains as discussed in ref 25.) The crossover between combs and bottlebrushes is defined by setting $\Phi_1 \approx 1$ and solving eq 1 for composition parameter as a function $n_{sc,1}$

$$\varphi_1^{-1} \approx \nu^{-1}(bl)^{3/2} n_{sc,1}^{1/2} \tag{3}$$

This crossover expression is shown as a solid black line in Figure 2 representing the different regimes of monodisperse

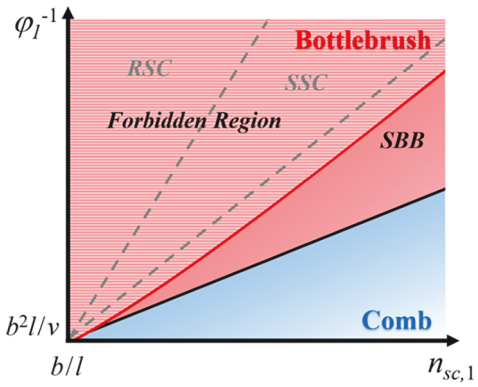

Figure 2. Diagram of states of graft polymers with monodisperse flexible side chains, $n_{sc,1} > b/l$, in a melt. SBB—stretched backbone subregime, SSC—stretched side chain subregime, and RSC—rod-like side chain subregime. The accessible regimes of the diagram of states are determined by the chemistry of the backbone which restricts the maximum number of side chains n_g^{max} per backbone monomer. Because of this constraint, the upper boundary of accessible regimes is given by $\varphi_1^{-1} \le \varphi_{max}^{-1} = n_{sc,1}/n_g^{max} + 1$, which is plotted for $n_g^{max} = 1$.

graft polymers in $n_{sc,1}$ and φ_1^{-1} coordinates. In the comb regime, the steric repulsion between side chains is weak and graft polymers can be considered as unperturbed ideal chains with the effective Kuhn length being equal to that of the backbones.

$$b_1 \approx b \tag{4}$$

In the bottlebrush regime (see Figure 2), the value of the crowding parameter is $\Phi_1 > 1$. Note that the unphysical value of the crowding parameter $\Phi_1 > 1$ corresponds to a hypothetical system where backbones and side chains maintain their ideal conformations even in the case of macromolecules with densely grafted side chains. Thus, in the real systems to preserve monomer density $\rho \approx \nu^{-1}$, the backbone stretches to decrease the number of side chains within the volume $R_{sc,1}^3$. This subregime is called stretched backbone (SBB) subregime in Figure 2 to emphasize stretching of the backbone due to steric repulsion between side chains. Note that this regime is a dominant regime of bottlebrushes. From the packing condition ($\rho\nu \approx 1$), the number of backbone monomers g within the volume $R_{sc,1}^3$ decreases with increasing crowding parameter Φ_1 as

$$g\varphi_1^{-1} \cdot \nu R_{sc,1}^{-3} \approx g\Phi_1/n_{sc,1} \approx 1 \tag{5}$$

On the length scales larger than the side chain size, a bottlebrush can be considered as a flexible chain of blobs each of size $R_{sc,1}$ and with the effective Kuhn length

$$b_1 \equiv R_e^2/Nl \approx R_{sc,1}^2 N/gNl \approx b\Phi_1 \tag{6}$$

Crossover to a new subregime takes place when the section of the backbone consisting of g monomers becomes fully extended such that $gl \approx R_{sc,1}$. This condition is satisfied for

$$\varphi_1^{-1} \approx \nu^{-1} bl^2 n_{sc,1} \tag{7}$$

which determines the upper boundary of the stretched side chains (SSC) subregime in Figure 2. Above this line, the side chains begin to stretch to maintain the constant density in a melt, $\rho\nu \approx 1$ (SSC subregime in Figure 2). Taking into account the packing condition

$$R_{sc,1}\varphi_1^{-1} \cdot \nu/lR_{sc,1}^3 \approx \nu\varphi_1^{-1}/lR_{sc,1}^2 \approx 1 \tag{8}$$

and solving for the size of side chains, we have

$$R_{sc,1} \approx (\nu/\varphi_1 l)^{1/2} \tag{9}$$

The effective Kuhn length of bottlebrushes in the SSC subregime is

$$b_1 \approx R_{sc,1} \approx (\nu/\varphi_1 l)^{1/2} \tag{10}$$

Finally, the side chains become fully stretched, $R_{sc,1} \approx ln_{sc,1}$, for

$$\varphi_1^{-1} \approx \nu^{-1} l^3 n_{sc,1}^2 \tag{11}$$

Above this line, both side chains and backbones are fully stretched on length scales smaller than the side chain size $R_{sc,1}$. The effective Kuhn length of bottlebrushes in this regime is equal to $b_1 \approx l\, n_{sc,1}$. This regime is called rod-like side chain (RSC) subregime in the diagram of states in Figure 2. Table 1 summarizes the regime boundaries and expressions for the effective Kuhn length in the different conformational regimes.

Specificity of the chemical structure of the graft polymers sets the maximum number of side chains which is possible to graft to a backbone monomer $1/n_g^{max}$. This imposes an upper

Table 1. Conformational Regimes Shown in Figure 2 and the Corresponding Effective Kuhn Lengths of Graft Polymers with Flexible Side Chains

Regime		Regime boundaries[a]	Kuhn length, b_1
Comb, $\Phi_1<1$		$\nu\varphi_1^{-1} \le (bl)^{3/2} n_{sc,1}^{1/2}$	b
Bottlebrush, $\Phi_1>1$	SBB	$(bl)^{3/2} n_{sc,1}^{1/2} \le \nu\varphi_1^{-1} \le bl^2 n_{sc,1}$	$\nu l^{-3/2} b^{-1/2} \varphi_1^{-1} n_{sc,1}^{-1/2}$
	SSC	$bl^2 n_{sc,1} \le \nu\varphi_1^{-1} \le l^3 n_{sc,1}^2$	$\nu^{1/2} l^{-1/2} \varphi_1^{-1/2}$
	RSC	$l^3 n_{sc,1}^2 \le \nu\varphi_1^{-1}$	$ln_{sc,1}$

[a] l—monomer projection length, b—Kuhn length of a linear polymer chain, and ν—monomer excluded volume.

https://dx.doi.org/10.1021/acs.macromol.0c02610
Macromolecules 2021, 54, 1818−1828

boundary $\varphi_1^{-1} \le \varphi_{1,\max}^{-1} = n_{sc,1}/n_g^{max} + 1$ on the accessible regimes in the diagram of states in Figure 2.

Diagram of States of Graft Polymers with Bimodal Distribution of Side Chains. In describing conformations of graft polymers with two different types of side chains we take into account that steric repulsions between short side chains and sections of the long side chains close to the backbone with the DP comparable to $n_{sc,1}$ renormalize the backbone Kuhn length to b_1 (see Table 1). The blob structure in this case is illustrated in Figure 1c. This additional stiffening of the backbone requires consideration of two different cases of longer side chains whose size, $R_{sc,2} \approx (bln_{sc,2})^{1/2}$, could be larger or smaller than the effective Kuhn length of the backbone b_1. Note that the situation is similar to the case of graft polymers with backbones and side chains made of different types of monomers. Equating the size of the longer side chains $R_{sc,2} \approx (bln_{sc,2})^{1/2}$with the effective Kuhn length of the backbone b_1, we obtain the following expression for the crossover value of the DP of the side chains

$$n_{sc,2} \approx b_1^2/bl \tag{12}$$

For side chains with DP $n_{sc,2} < b_1^2/bl$, the backbones of graft polymers are rod-like on the length scales on the order of the side chain size and contain $g \approx R_{sc,2}/l$ backbone monomers. In this case, the crowding parameter, determining crossover between comb and bottlebrush states, is estimated as

$$\Phi \approx g\varphi^{-1}\cdot v/R_{sc,2}^3 \approx vl^{-2}b^{-1}\varphi^{-1}n_{sc,2}^{-1}, \quad \text{for } n_{sc,1} < n_{sc,2} \le b_1^2/bl \tag{13}$$

where we introduced graft polymer composition parameter

$$\varphi = (1 + (fn_{sc,1} + (1-f)n_{sc,2})/n_g)^{-1} \tag{14}$$

In the case of flexible backbones on the length scale of the longer side chains, $n_{sc,2} > b_1^2/bl$, the number of backbone monomers within the size of the side chains, $R_{sc,2}$, is on the order of $g \approx n_{sc,2}b/b_1$and the crowding parameter is written as

$$\Phi \approx vl^{-3/2}b_1^{-1}b^{-1/2}\varphi^{-1}n_{sc,2}^{-1/2}, \qquad \text{for } n_{sc,2} > b_1^2/bl \tag{15}$$

Crossover conditions between comb and bottlebrush regimes are obtained by setting the value of the crowding parameter in eqs 13 and 15 to unity and solving these equations for the composition parameter

$$\varphi^{-1} \approx v^{-1}l^{3/2}b^{1/2}\begin{cases} b_1 n_{sc,2}^{1/2}, & \text{for } n_{sc,2} > b_1^2/bl \\ (bl)^{1/2}n_{sc,2}, & \text{for } n_{sc,1} < n_{sc,2} \le b_1^2/bl \end{cases} \tag{16}$$

Figure 3 presents the diagram of states and Table 2 summarizes the regime boundaries and dependence of the graft polymer Kuhn length on its composition. This diagram of states is constructed for fixed n_g and $n_{sc,1}$ which determine backbone effective rigidity reflected in its effective Kuhn length b_1. Note that in writing down boundaries of different regimes we take into account that the graft polymer composition parameter changes within the envelop

$$(1 + n_{sc,2}/n_g)^{-1} = \varphi_2 \le \varphi \le \varphi_1 \tag{17}$$

and the DP of the longer chains satisfies the inequality $n_{sc,2} > n_{sc,1}$. We discarded the RSC subregime since it occupies an insignificant region of the diagram of states.

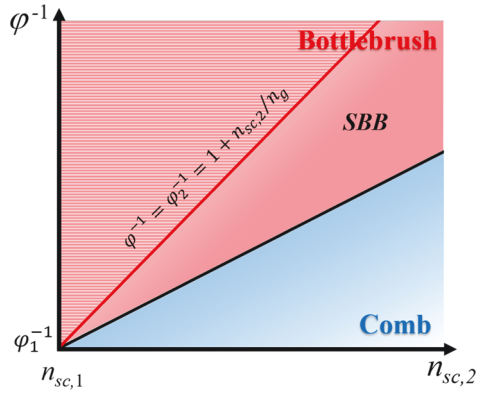

Figure 3. Diagram of states of graft copolymers with bimodal distribution of the side chains in a melt, for $\Phi_1 > 1$. The black solid line is a boundary between comb and bottlebrush (SBB) regimes, and the red line shows upper boundary of the accessible region.

COMPARISON WITH SIMULATIONS

Coarse-grained MD simulations were performed to test the scaling model of graft polymers with a bimodal distribution of the side chains in a melt.[24,25] Graft macromolecules were represented by bead-spring chains made of beads with diameter σ. All beads in a system interacted through modified truncated-shifted Lennard-Jones (LJ) potentials. The connectivity of the beads into backbones and side chains was maintained by the finite extensible nonlinear elastic (FENE) bonds.[32] The explicit form of the interaction potentials is given in the Methods section below. Each graft copolymer consisted of a linear chain backbone with the number of monomers N_{bb} = 130 and grafted side chains having $n_{sc,1}$ and $n_{sc,2}$ monomers with n_g/f and $n_g/(1-f)$ backbone bonds between nearest grafting points of the similar side chains (Figure 1). Table 3 summarizes the studied systems and shows symbols used to represent simulation results.

Bond−Bond Correlation Function. We first study the effect of different types of side chains and their composition on the effective Kuhn length. The stiffening of the backbones induced by steric repulsion between side chains is quantified by analyzing the bond−bond correlation function of the backbones, $G(s)$. This function describes the decay of the orientational correlations between two unit backbone bond vectors $\mathbf{n}_i$ and $\mathbf{n}_{i+s}$ separated by s bonds and is defined as follows[24]

$$G(s) = \frac{1}{N_{bb} - s}\sum_{i=1}^{N_{bb}-s} \langle \mathbf{n}_i \cdot \mathbf{n}_{i+s} \rangle \tag{18}$$

where the brackets $\langle ... \rangle$ represent the ensemble average over the backbone conformations during simulation runs. The end chain effects were minimized by neglecting contribution from 20 bonds on both backbone ends in calculations of the function $G(s)$. Figure 4 shows typical bond−bond correlation functions of graft copolymers with different fractions f of the side chains and their DPs. As expected, with the increasing fraction of the longer side chains, the graft polymers stiffen. The effect of the backbone stiffening is quantified by fitting the simulation results to a sum of two exponential functions[21,24]

$$G(s) = (1-\alpha)\exp\left(-\frac{|s|}{\lambda_1}\right) + \alpha \exp\left(-\frac{|s|}{\lambda_2}\right) \tag{19}$$

https://dx.doi.org/10.1021/acs.macromol.0c02610
Macromolecules 2021, 54, 1818−1828

Table 2. Effective Kuhn Length of Graft Polymers with Two Types of Side Chains in Different Regimes and Regime Boundaries

Regime		Regime boundaries	Kuhn length, b_K
Comb, Φ<1		$v\varphi_1^{-1} \le v\varphi^{-1} \le l^{3/2}b^{1/2}b_1 n_{sc,2}^{1/2}$, for $b_1^2/bl \le n_{sc,2}$ $v\varphi_1^{-1} \le v\varphi^{-1} \le l^2 b n_{sc,2}$, for $n_{sc,1} \le n_{sc,2} \le b_1^2/bl$	b_1
Bottlebrush, Φ>1	SBB	$l^{3/2}b^{1/2}b_1 n_{sc,2}^{1/2} \le v\varphi^{-1} \le l^2 b n_{sc,2}$	$vl^{-3/2}b^{-1/2}\varphi^{-1}n_{sc,2}^{-1/2}$
	SSC	$l^2 b n_{sc,2} \le v\varphi^{-1} \le v\varphi_2^{-1}$ and $b_1^2 l \le v\varphi^{-1}$ $l^2 b n_{sc,2} \le v\varphi^{-1} \le b_1^2 l$ and $\varphi^{-1} \le \varphi_2^{-1}$	$(v/\varphi l)^{1/2}$ b_1

where α, λ_1, and λ_2 are fitting parameters. This functional form captures two mechanisms of the induced chain rigidity on different length scales with corresponding correlation lengths λ_1 and λ_2. At short length scales, the rigidity of the backbone is due to local backbone tension, while at long length scales, it is a result of interactions between neighboring side chains.

Effective Kuhn Length. The backbone bond−bond correlation function was used to calculate the mean-square end-to-end distance of a backbone section with s bonds

$$\langle R_e^2(s)\rangle = \frac{1}{N_{bb}-s+1}\sum_{i=1}^{N_{bb}-s+1}\left\langle l^2\left(\sum_{j=i}^{i+s-1}\mathbf{n}_j\right)^2\right\rangle \tag{20}$$

where l is the bond length. The effective Kuhn length b_K of graft polymers is expressed in terms of the fitting parameters of the bond−bond correlation as follows[24,33]

$$b_K = \left.\frac{\langle R_e^2(s)\rangle}{sl}\right|_{s\to\infty} = l((1-\alpha)h(\lambda_1) + \alpha h(\lambda_2)) \tag{21}$$

where function $h(\lambda)$ is given by

$$h(\lambda) = \frac{1+e^{-1/\lambda}}{1-e^{-1/\lambda}} \tag{22}$$

The results of these calculations are summarized in Figure 5a, showing the dependence of the effective Kuhn length of graft polymers on the crowding parameter Φ. In the comb regime for longer side chains, the graft polymer Kuhn length is controlled by the short side chains which renormalize the backbone Kuhn length to b_1. With an increasing fraction of the longer side chains $(1-f)$, the longer side chains increase backbone stiffening, resulting in a linear scaling of the effective Kuhn length with crowding parameter Φ. Figure 5b shows the collapse of the data for the mean square end-to-end distance of the section of the backbone with n bonds, $\langle R_{e,bb}^2(n)\rangle$, normalized by square of the effective Kuhn length, b_K^2, as a function of normalized contour length nl/b_K. The stronger than linear growth of the mean square average end-to-end size of the section of the backbone for $nl/b_K < 1$indicates that at length scales smaller than effective backbone Kuhn length b_K, sections of the backbone are stretched. However, for $nl/b_K \gg 1$, graft polymer backbones demonstrate ideal chain behavior with Kuhn length b_K.

Diagrams of States. Figure 6 shows diagrams of states for the simulated systems. To obtain regime boundaries, we take into account that in a crossover between Comb and Bottlebrush regimes (see Figure 5a) the value of the crowding parameter $\Phi \approx \Phi^* \cong 0.7$ and use this correction to rewrite eq 16 for φ^{-1} as a function of the side chain DPs. Figure 6 illustrates two projection classifications of the graft polymers with a bimodal distribution of the side chains. Thus, to classify different conformational regimes of graft polymers, we have to use dual notations (comb, comb), (bottlebrush, comb), and (bottlebrush, bottlebrush), depending on the values of corresponding crowding parameters Φ_1 and Φ to reflect different conformational regimes of graft polymers with a mixture of short and long side chains.

SCATTERING FROM MELTS OF GRAFT POLYMERS WITH BIMODAL DISTRIBUTION OF SIDE CHAINS

Scattering from melts of graft polymers provides an access to their conformational properties through analysis of the static structure factor $S(q)$ which is defined as follows

$$S(q) = \frac{1}{V}\sum_{i=1}^{N_b}\sum_{j=1}^{N_b} f_i f_j \langle \exp[-i\mathbf{q}\cdot(\mathbf{R}_i - \mathbf{R}_j)]\rangle \tag{23}$$

where $\mathbf{q}$ is the scattering vector, and f_i is the form factor of the i-th bead located at point with the radius vector $\mathbf{R}_i$. Summation in eq 23 is carried out over all (monomers) beads N_b in a system and brackets $\langle\rangle$ denote ensemble averaging.

Calculations of function $S(q)$ in the framework of the RPA[34−37] allow for direct evaluation of the elements $G_{\alpha\beta}(q)$ of the matrix of pair correlation functions $\mathbf{G}(q)$ describing correlations in density fluctuations of monomers of types α and β[38,39]

$$S(q) = f_\alpha f_\beta \langle \delta\rho_\alpha(q)\delta\rho_\beta(-q)\rangle = f_\alpha f_\beta G_{\alpha\beta}(q) \tag{24}$$

where summation over repeating indexes is used and $\alpha = s$ corresponds to monomers of the side chains while $\alpha = b$ represents those of the backbones. In this approximation, the matrix $\mathbf{G}(q)$ of the pair correlation functions is written in terms of the matrix of structural correlation functions $\mathbf{g}(q)$ describing the arrangement of monomers into macromolecules and the matrix of the direct correlation functions $\mathbf{C}(q)$ characterizing interactions between monomers[34−36,38,40]

$$\mathbf{G}^{-1}(q) = \mathbf{g}^{-1}(q) - \mathbf{C}(q) \tag{25}$$

Elements $g_{\alpha\beta}(q)$ of the matrix of structural correlation function are defined as

$$g_{\alpha\beta}(q) = \rho_M \sum_{i_\alpha=1}^{N_\alpha}\sum_{j_\beta=1}^{N_\beta}\langle \exp[-i\mathbf{q}\cdot(\mathbf{R}_{i_\alpha} - \mathbf{R}_{j_\beta})]\rangle \tag{26}$$

where ρ_M is the number density of graft polymers with a bimodal distribution of the side chains which is equal to

$$\rho_M = \rho/(n_{bb} + (fn_{sc,1} + (1-f)n_{sc,2}) \times (n_{bb} - (n_g+1))/n_g) \approx p\varphi/n_{bb} \tag{27}$$

https://dx.doi.org/10.1021/acs.macromol.0c02610
Macromolecules 2021, 54, 1818−1828

Table 3. Summary of Studied Systems and Symbol Notations

n_g	$n_{sc,1}$	$n_{sc,2}$	f	$b_K[\sigma]$	φ^{-1}	$\Phi^{*)}$	*Symbol*
1	8	32	0.0	7.79	33	1.26	
1	8	32	0.25	6.59	27	1.03	
1	8	32	0.5	6.14	21	0.80	
1	8	32	0.75	5.31	15	0.57	
1	8	32	1.0	4.22	9	1.46	
1	16	32	0.0	7.79	33	0.90	
1	16	32	0.25	7.62	29	0.79	
1	16	32	0.5	7.16	25	0.68	
1	16	32	0.75	6.06	21	0.57	
1	16	32	1.0	5.92	17	1.95	
2	8	32	0.0	4.30	17	0.96	
2	8	32	0.25	3.81	14	0.79	
2	8	32	0.5	3.45	11	0.62	
2	8	32	0.75	3.24	8	0.45	
2	8	32	1.0	2.84	5	0.81	
2	16	32	0.0	4.30	17	0.75	
2	16	32	0.25	3.95	15	0.66	
2	16	32	0.5	3.86	13	0.57	
2	16	32	0.75	3.74	11	0.48	
2	16	32	1.0	3.65	9	1.03	
4	8	32	0.0	2.87	9	0.62	
4	8	32	0.25	2.69	7.5	0.51	
4	8	32	0.5	2.64	6	0.41	
4	8	32	0.75	2.47	4.5	0.31	
4	8	32	1.0	2.35	3	0.49	
4	16	32	0.0	2.87	9	0.57	
4	16	32	0.25	2.79	8	0.51	
4	16	32	0.5	2.82	7	0.44	
4	16	32	0.75	2.82	6	0.38	
4	16	32	1.0	2.53	5	0.57	
8	8	32	0.0	2.31	5	0.38	
8	8	32	0.25	2.30	4.25	0.32	
8	8	32	0.5	2.22	3.5	0.27	
8	8	32	0.75	2.18	2.75	0.21	
8	8	32	1.0	2.12	2	0.32	
8	16	32	0.0	2.31	5	0.36	
8	16	32	0.25	2.32	4.5	0.33	
8	16	32	0.5	2.27	4	0.29	
8	16	32	0.75	2.28	3.5	0.25	
8	16	32	1.0	2.22	3	0.34	
16	8	32	0.0	2.14	3	0.24	
16	8	32	0.25	2.11	2.625	0.21	
16	8	32	0.5	2.07	2.25	0.18	
16	8	32	0.75	2.07	1.875	0.15	
16	8	32	1.0	2.04	1.5	0.24	
16	16	32	0.0	2.14	3	0.23	
16	16	32	0.25	2.11	2.75	0.21	
16	16	32	0.5	2.08	2.5	0.19	
16	16	32	0.75	2.08	2.25	0.17	
16	16	32	1.0	2.09	2	0.23	

*)Value of the crowding parameter are calculated as $\Phi = \Phi_1 \approx \nu(lb)^{-3/2}\varphi_1^{-1}n_{sc,1}^{-1/2}$ for $f = 1.0$, and $\Phi \approx \nu l^{-3/2}b_1^{-1}b^{-1/2}\varphi^{-1}n_{sc,2}^{-1/2}$ for $f \neq 1.0$ using the following values for $l = 0.985\sigma$, $b = 1.98\sigma$, and $\nu = 1/\rho = 1.25\sigma^3$. Graft polymer composition is defined as $\varphi^{-1} = 1 + (fn_{sc,1} + (1 - f)n_{sc,2})/n_g$.

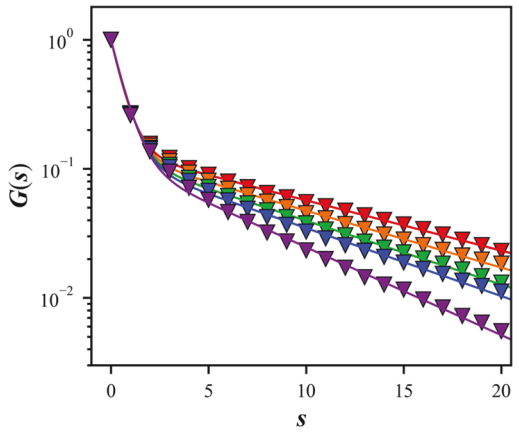

Figure 4. Bond−bond correlation functions $G(s)$ of graft polymer backbones for graft polymers characterized by structural quadruplets (n_g, $n_{sc,1}$, $n_{sc,2}$, f): (2, 8, 32, 0) (red inverted triangles), (2, 8, 32, 0.25) (orange inverted triangles), (2, 8, 32, 0.5) (green inverted triangles), (2, 8, 32, 0.75) (blue inverted triangles), and (2, 8, 32, 1.0) (purple inverted triangles). The lines are the best fits to eq 19.

The summation in eq 26 is carried out over all monomers of types α and β located at points with radius vectors $\mathbf{R}_{i_\alpha}$ and $\mathbf{R}_{j_\beta}$, and brackets $\langle\rangle$ denote averaging over conformations of graft polymers. The functions $g_{\alpha\beta}(q)$ are proportional to intrachain correlation functions with proportionality coefficient being number density of macromolecules. The specific form of the matrix $\mathbf{C}(\mathbf{q})$ depends on the model used to describe monomer−monomer interactions.

For incompressible melts, the local density fluctuations should satisfy the incompressibility condition such that the density fluctuations of the monomers belonging to the side chains are offset by those from the backbones, $\delta\rho_s(q) = -\delta\rho_b(q)$. Taking this into account, the expression for the scattering function reduces to

$$S(q) = (f_s - f_b)^2\langle\delta\rho_s(q)\delta\rho_s(-q)\rangle = (f_s - f_b)^2 \times (g_{ss}^{-1}(q) + g_{bb}^{-1}(q) - 2g_{sb}^{-1}(q) - 2\nu\chi)^{-1} \quad (28)$$

where $g_{\alpha\beta}^{-1}(q)$ are matrix elements of the inverse matrix $\mathbf{g}^{-1}(q)$, and $\chi = \nu(\delta_s - \delta_b)^2/2k_BT$ is the Flory−Huggins parameter for monomers belonging to side chains and backbones expressed in terms of the solubility parameters δ_α of a bead type α. In obtaining this expression, we used the lattice model to describe monomer−monomer interactions.

There are two main building blocks in the expression of the structural correlation functions $g_{\alpha\beta}(q)$: (i) correlation function for monomers belonging to the same block and (ii) correlation function for monomers belonging to different blocks as illustrated in Figure 7. Here, we call blocks either side chains or sections of the backbone between two grafted side chains. Below, we will briefly describe calculations of the structural correlation functions for graft polymers with two different types of side chains following formalism developed in ref 20.

Comb Regime. In this regime, conformations of the side chains and backbones are those of the ideal (Gaussian) chains and the contribution from each bond to the correlation functions can be approximated as that from a spring with spring constant $3k_BT/lb$.[20,36,41] In this approximation, the

https://dx.doi.org/10.1021/acs.macromol.0c02610
Macromolecules 2021, 54, 1818−1828

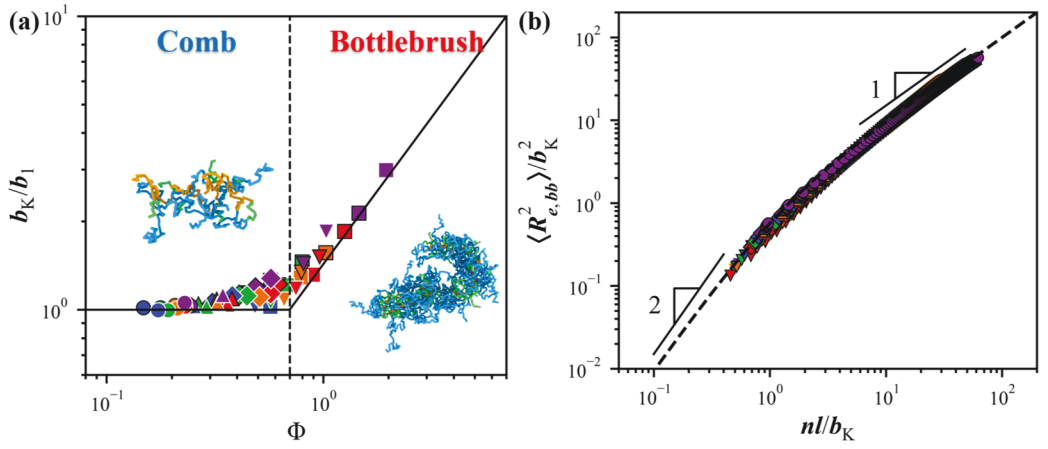

Figure 5. (a) Dependence of the reduced Kuhn length, b_K/b_1, of graft polymers with bimodal distribution of the side chains on the crowding parameter, Φ. Values of the crowding parameter are calculated as $\Phi = \Phi_1 \approx \nu(lb)^{-3/2}\varphi_1^{-1}n_{sc,1}^{-1/2}$ for $f = 1.0$, and $\Phi \approx \nu l^{-3/2}b_1^{-1}b^{-1/2}\varphi^{-1}n_{sc,2}^{-1/2}$ for $f \neq 1.0$ using the following values for $l = 0.985\sigma$, $b = 1.98\sigma$, and $\nu = 1/\rho = 1.25\sigma^3$. Kuhn length b_1 is the effective Kuhn length of the graft polymers with monodisperse side chains $n_{sc,1}$ and grafting density $1/n_g$. Comb and Bottlebrush regimes refer to regime classification for the long side chains. (b) Dependence of the normalized mean-square end-to-end distance of the section of the graft polymer backbone with n bonds on the number of Kuhn segments. The dashed line corresponds to the worm-like chain model. See Table 3 for symbol notations.

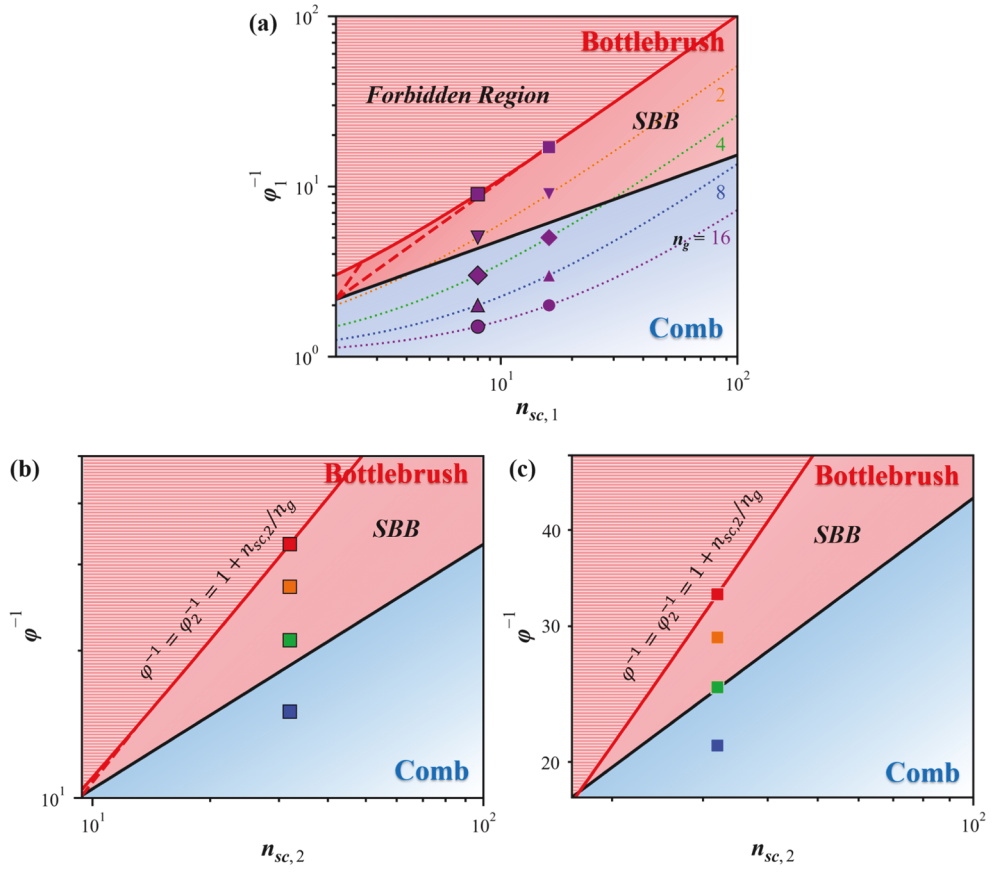

Figure 6. Diagrams of states of graft polymers with bimodal distribution of the side chains. (a) Diagram of states of graft polymers with short side chains only and different grafting densities. (b,c) Diagrams of states of graft polymers with $n_g = 1$, short side chain DPs 8 and 16, and long side chains DP equal to 32.

intrablock structural correlation function for a block with the DP n is given by the Debye function in the limit $q^2lb \ll 1$

$$g_n(q) \approx 2n^2\frac{\exp(-q^2R_n^2) + q^2R_n^2 - 1}{(q^2R_n^2)^2} \quad (29)$$

where $R_n^2 \equiv lbn/6$ was introduced. The intrablock correlation function with one point fixed at the grafting point of the block has the following form

$$\xi_n(q) \approx n\frac{1 - \exp(-q^2R_n^2)}{q^2R_n^2} \quad (30)$$

https://dx.doi.org/10.1021/acs.macromol.0c02610
Macromolecules 2021, 54, 1818−1828

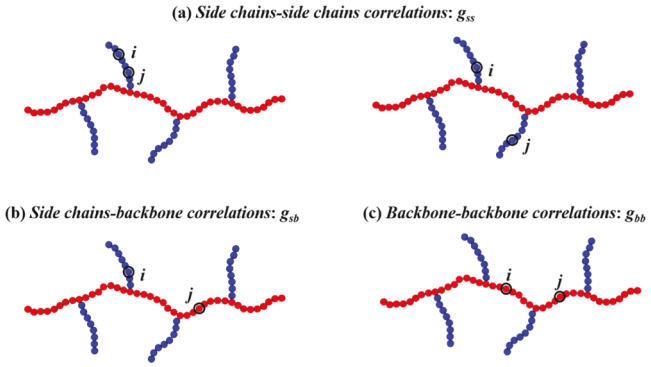

Figure 7. Schematic diagram used in the calculation of the structural correlation functions. Adapted from ref 20. Copyright ACS 2019.

The structural correlation functions of graft polymers with the number of side chains $N_{sc} = (n_{bb} - (n_g + 1))/n_g$ are built on the functions eqs 29 and 30 modified with summations over the separating blocks. The structural correlation functions of graft polymers, in the limit of the large number of the side chains $N_{sc} \approx N_{bb}/n_g \gg 1$ and the interval of wave numbers $q^2 l \ll 1$, are written as follows

$$g_{ss}(q) \approx \rho_M N_{sc}\left(\langle g_{n_{sc}}(q)\rangle + \frac{2\langle \xi_{n_{sc}}(q)\rangle^2 \exp(-q^2 R_{n_g}^2)}{1 - \exp(-q^2 R_{n_g}^2)}\right);$$

$$g_{bb}(q) \approx \rho_M N_{sc} \frac{2n_g^2}{q^2 R_{n_g}^2};\ g_{sb}(q) \approx \rho_M N_{sc} \frac{2n_g \langle \xi_{n_{sc}}(q)\rangle}{q^2 R_{n_g}^2} \quad (31)$$

where functions

$$\langle g_{n_{sc}}(q)\rangle = f g_{n_{sc,1}}(q) + (1-f) g_{n_{sc,2}}(q) \quad (32)$$

$$\langle \xi_{n_{sc}}(q)\rangle = f \xi_{n_{sc,1}}(q) + (1-f) \xi_{n_{sc,2}}(q) \quad (33)$$

reflect averaging over two different types of side chains distributed along the polymer backbones.

To illustrate how polydispersity of the side chains changes the results obtained for graft polymers with monodisperse side chains, we first consider a dilute side chain regime, where the

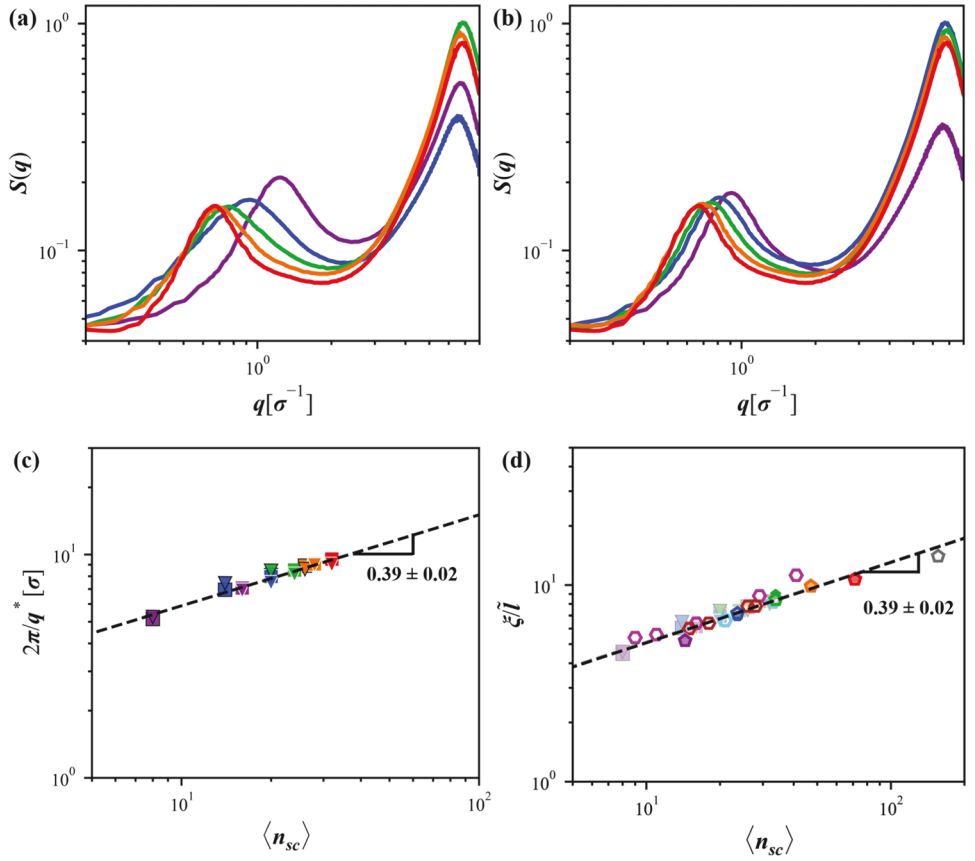

Figure 8. Static structure factor $S(q)$ in melts of graft polymers for different fractions of short side chains f and with (a) $n_g = 1$, $n_{sc,1} = 8$, and $n_{sc,2} = 32$ and (b) $n_g = 1$, $n_{sc,1} = 16$, and $n_{sc,2} = 32$. Lines with different colors correspond to $f = 1$ (purple), 0.75 (blue), 0.5 (green), 0.25 (orange), and 0 (red). (c) Dependence of the characteristic length scale $\xi = 2\pi/q^*$ corresponding to the peak position, q^*, on the number average DP of the side chains $\langle n_{sc}\rangle = f n_{sc,1} + (1-f) n_{sc,2}$ for bottlebrushes with $n_g = 1$ and 2. Symbol notations are given in Table 3. (d) Dependence of normalized characteristic length scale $\xi/\tilde{l}$ ($\tilde{l} = (bl)^{1/8} v^{1/4}$) on the number average DP of the side chains $\langle n_{sc}\rangle$ for the simulation data in panel (c) (shown by light colored symbols in the background) and experimental data sets for bottlebrushes with flexible acrylate backbone[44] (open magenta hexagons), single arm rigid norbornene backbone[44] (open cyan hexagons), and double-arm rigid norbornene backbone[44] (open brown hexagons) and for bottlebrush blocks of poly(dimethylsiloxane)-methacrylate linear-bottlebrush-linear plastomers[47] with bimodal distribution of side chains ($n_g = 1$, $n_{sc,1} = 14$, $n_{sc,2} = 71$) and fractions of side chains $f = 1$ (open purple pentagons), 0.84 (open blue pentagons), 0.66 (open green pentagons), 0.42 (open orange pentagons), 0 (open red pentagons), and poly(dimethylsiloxane) bottlebrushes[47] with $n_{sc} = 156$ (grey open pentagon). Experimental data are superimposed with simulation results by using shift factors $\tilde{l} = 0.5$ nm and 0.65 nm for data sets from refs 44 and 47, respectively.

https://dx.doi.org/10.1021/acs.macromol.0c02610
Macromolecules 2021, 54, 1818−1828

distance between grafting points of the side chains $\langle R_e^2(n_g)\rangle^{1/2} = \sqrt{lbn_g}$ is larger than the size of both short $\langle R_e^2(n_{sc,1})\rangle^{1/2} = \sqrt{lbn_{sc,1}}$ and long $\langle R_e^2(n_{sc,2})\rangle^{1/2} = \sqrt{lbn_{sc,2}}$ side chains. Substituting corresponding approximations for the side chain block functions given by eqs 29 and 30 into eq 31 and taking into account that $q^2R_{n_g}^2 \gg 1$one obtains

$$g_{ss}^{C}(q) \approx \rho_M N_{sc}\frac{12\langle n_{sc}\rangle}{q^2lb};\ g_{bb}^{C}(q) \approx \rho_M N_{sc}\frac{12n_g}{q^2lb};$$
$$g_{sb}^{C}(q) \approx \rho_M N_{sc}\frac{72}{q^4l^2b^2} \tag{34}$$

where the number average side-chain DP is equal to

$$\langle n_{sc}\rangle = fn_{sc,1} + (1-f)n_{sc,2} \tag{35}$$

The peak position q^* in the scattering function $S(q)$ corresponds to the minimum of the function

$$\min\left[\frac{g_{ss}(q) + g_{bb}(q) - 2g_{sb}(q)}{g_{ss}(q)g_{bb}(q) - g_{sb}^2(q)}\right] \tag{36}$$

where we use the explicit form of the elements of the inverse matrix $\mathbf{g}^{-1}(q)$. Taking the derivative of the expression in brackets in eq 36 with respect to q^2 and solving it for q, we find that the peak position scales with the system parameters as

$$q^* \approx (R_{n_g}R_{\langle n_{sc}\rangle})^{-1/2} \propto (n_g\langle n_{sc}\rangle)^{-1/4} \tag{37}$$

Thus, the peak position shifts toward small q-values with side chain dilution (increasing the DP of the spacer between side chains) and increasing DP of side chains.

Bottlebrush Regime. In this regime, interactions between side chains stiffen the backbone, increasing its Kuhn length from the bare value b to $b_K \approx b\Phi/\Phi^*$ with increasing value of the crowding parameter above its crossover value Φ^*.[24] It is important to point out that eq 31 can also be used to describe structural correlations of bottlebrush macromolecules in the interval of wave numbers, $qb_K < 1$, where the bottlebrushes can be approximated by flexible chains with the effective Kuhn length equal to b_K. In this case, inter-side chain correlation functions are given by eq 31 and the backbone−backbone correlation function is approximated by the Debye function.[42] Substituting $R_{n_g}^2 = lb_Kn_g/6$ and $R_{\langle n_{sc}\rangle}^2 = lb\langle n_{sc}\rangle/6$ into eq 31, the structural correlation functions of the bottlebrush systems can be written as

$$g_{ss}^{B}(q) \approx 12\rho_M N_{sc}\left(\frac{\langle n_{sc}\rangle}{q^2lb} + \frac{36b}{n_gb_K}\frac{1}{(q^2lb)^3}\right);$$
$$g_{bb}^{B}(q) \approx 12\rho_M N_{sc}\frac{n_g}{q^2lb_K};\ g_{sb}^{B}(q) \approx 72\rho_M N_{sc}\frac{b}{b_K}\frac{1}{(q^2lb)^2} \tag{38}$$

where superscript index "B" stands for bottlebrush. In this approximation, the location of the peak is

$$q^* \approx 6^{1/2}(n_g\langle n_{sc}\rangle bb_Kl^2)^{-1/4} \propto \langle n_{sc}\rangle^{-3/8} \tag{39}$$

This expression is similar to eq 37 where the renormalized value of the backbone Kuhn length b_K is substituted into the expression for R_{n_g} instead of its bare value b. This is a weaker dependence than one expected for this length scale to be associated with the inter backbone distance, $q^* \propto \langle n_{sc}\rangle^{-0.5}$.[43−45]

Computer Simulations of Scattering. To calculate the structure factor of graft polymer with a bimodal distribution of side chains in coarse-grained MD simulations, the monomer form factors were set to $f_b = 1.5$ for the backbone beads and $f_s = 1.0$ for the side chain beads. In our calculations of the structure factor, we have adapted the fast Fourier transform-based approach developed in ref 46. In this representation, the actual beads are assigned to the regular grid points with weights proportional to their distances.

Figure 8a,b shows typical scattering curves for graft polymers with a bimodal distribution of the side chains. There are two clearly identifiable peaks in the static structure factor. The high q-peak corresponds to correlations between those neighboring along the side chain and backbone monomers. The location of this peak does not move with changing fraction of the side chains. The second peak (q^* peak) located at low q-range changes position with the increasing fraction of the long side chains. It moves toward lower q-values as the fraction of the longer side chains increases. This is in agreement with a trend expected from the scaling relation predicted by eq 39. Figure 8c quantifies this scaling relation by plotting dependence of the characteristic length scale $2\pi/q^*$ as a function of the number average DP of the side chains $\langle n_{sc}\rangle$. All data points collapse into one universal line as expected from eq 39 with a slightly stronger scaling dependence $2\pi/q^* \propto \langle n_{sc}\rangle^{0.39\pm0.02}$. In Figure 8d, we plot together simulation and experimental data for bottlebrushes with monodisperse[44] and bimodal[47] side-chain distributions. We used constant shift factors to superimpose simulation and experimental data sets, which does not change the power-law scaling. There is an excellent agreement between data sets confirming the origin of the scattering peak.

CONCLUSIONS

We showed that the graft polymer with a bimodal distribution of the side chains can be described by approximating them as macromolecules with effective backbones made of graft polymers with short side chains to which long side chains are attached. This approximation allowed us to construct a diagram of states by using two two-dimensional projections as illustrated in Figures 2 and 3. In the framework of this approach, dual notations (comb, comb), (bottlebrush, comb), and (bottlebrush, bottlebrush) characterize different conformational regimes of such graft polymers. This representation was also used to extend the definition of the crowding parameter Φ and was applied to express effective Kuhn length in terms of the crowding parameter. Note that the developed approach requires a sufficient separation of the side chain degrees of polymerization. Developed frameworks are tested by coarse-grained MD simulations of the graft polymers with bimodal side-chain distribution in a melt. In particular, we analyze data for the effective Kuhn length (Figure 5) in terms of the crowding parameter and use crossover value of the crowding parameter to construct the diagram of states in Figure 6. To make a connection to experiments, we have calculated static structure factor $S(q)$ and show that the peak position in $S(q)$ can be expressed in terms of the number average DP of the side chains. In the bottlebrush regime, our simulation data for peak position q^* are independent of n_g and follow a scaling dependence $\langle n_{sc}\rangle^{-0.39\pm0.02}$ which is close to $\langle n_{sc}\rangle^{-0.375}$predicted by eq 39 (Figure 8c). The simulation results are in good agreement with experimental data as illustrated in Figure

https://dx.doi.org/10.1021/acs.macromol.0c02610
Macromolecules 2021, 54, 1818−1828

8d.[44,47] Note that this scaling dependence is weaker than one advocated in refs .[43−45] to be related with the inter backbone distances, $q^* \propto \langle n_{sc} \rangle^{-0.5}$. Furthermore, the derived expression for the static structure factor can be used for the analysis of scattering data from graft polymer systems.

METHODS

We perform MD simulations[48] of grafted comb-like polymers (combs) and bottlebrushes with two different types of side chains in a melt (see Figure 1). Each comb or bottlebrush polymer consists of a linear backbone chain with the number of monomers $N_{bb} = 130$ and two different types of side chains, short side chain $n_{sc,1}$ and long side chain $n_{sc,2}$, grafted to the backbone with n_g backbone bonds between the nearest grafting points of the side chains. In our simulations, the number fraction of short side chain, f, varies between 0 and 1 for $n_{sc,1} = 8$, 16 and $n_{sc,2} = 32$ with $n_g = 1$, 2, 4, 8, 16 (see Table 3). The grafting points of short side chains are evenly spaced along the backbone with the grafting density f/n_g.

Comb and bottlebrush macromolecules are modeled by the bead-spring chains made of beads with diameter σ. The interactions between monomers separated by distance r are described by the pure repulsive truncated-shifted LJ potential[32,48]

$$U_{LJ}(r) = \begin{cases} 4\varepsilon\left[\left(\frac{\sigma}{r}\right)^{12} - \left(\frac{\sigma}{r}\right)^{6} + \frac{1}{4}\right] & r \le 2^{1/6}\sigma \\ 0 & r > 2^{1/6}\sigma \end{cases} \quad (40)$$

where $\varepsilon = 1.5\ k_B T$ (where k_B is the Boltzmann constant and T is the absolute temperature). To describe the connectivity of beads into graft polymers, an additional FENE potential between neighboring beads

$$U_{FENE}(r) = -\frac{1}{2}kR_{max}^2 \ln\left(1 - \frac{r^2}{R_{max}^2}\right) \quad (41)$$

was applied with the spring constant $k = 30\ k_B T/\sigma^2$ and the maximum bond length $R_{max} = 1.5\sigma$. The repulsive part of the bond potential is modeled by the truncated-shifted LJ potential with $\varepsilon = 1.5\ k_B T$ and $r_{cut} = 2^{1/6}\sigma$. Simulations of combs and bottlebrushes with two different types of side chains were carried out in a constant volume with 3-D periodic boundary conditions at a constant temperature ensemble. The constant temperature was maintained by coupling the system to a Langevin thermostat implemented in LAMMPS.[49] In this representation, the equation of motion of the i-th bead is given by

$$m\frac{d\mathbf{v}_i(t)}{dt} = \mathbf{F}_i(t) - \xi\mathbf{v}_i(t) + \mathbf{F}_i^R(t) \quad (42)$$

where m is the mass of the bead, $\mathbf{v}_i(t)$ is the i-th bead velocity, $\mathbf{F}_i(t)$ is the net deterministic force acting on the i-th bead, and $\mathbf{F}_i^R(t)$ is the stochastic force with a zero average and a δ-function correlation $\langle \mathbf{F}_i^R(t)\cdot\mathbf{F}_j^R(t')\rangle = 6k_B T\xi\delta_{ij}\delta(t-t')$. The friction coefficient was set to $\xi = 0.1$ m/τ, where $\tau = \sigma\ (m/k_B T)^{1/2}$ is the standard LJ-time. The velocity−Verlet algorithm with a time step $\Delta t = 0.005\ \tau$ was used for integration of the equation of motion. All simulations were performed using LAMMPS.[49]

Simulations are performed in accordance with the following procedure.[20,24,25] $M = 100$ macromolecules are randomly placed in a simulation box with monomer number density equal to $0.8\sigma^{-3}$. To minimize the finite size effect for systems with $n_{sc} = 32$ and 16, the simulation box size was increased by a factor of 2 for systems with $n_g = 8$ and by a factor of 3 for systems with $n_g = 16$. A simulation run lasting 250 τ with the nonbonded interactions between beads turned off is performed in order to relax the initial macromolecule conformations. The strength of LJ-interaction parameter ε between beads is then gradually increased to $1.5k_B T$. This is followed by a simulation run continued until the mean square end-to-end distance of the backbones reach an equilibrium (saturates as a function of time). The equilibration run is followed by a product run lasting $5 \times 10^5\ \tau$ which is used for data collection.

AUTHOR INFORMATION

Corresponding Author

Andrey V. Dobrynin − *Department of Chemistry, University of North Carolina, Chapel Hill, North Carolina 27599, United States;* orcid.org/0000-0002-6484-7409; Email: avd@email.unc.edu

Authors

Haley Starvaggi − *School of Polymer Science and Polymer Engineering, University of Akron, Akron, Ohio 44325, United States*

Yuan Tian − *Department of Chemistry, University of North Carolina, Chapel Hill, North Carolina 27599, United States;* orcid.org/0000-0002-7277-1408

Heyi Liang − *Pritzker School of Molecular Engineering, University of Chicago, Chicago, Illinois 60637, United States;* orcid.org/0000-0002-8308-3547

Complete contact information is available at: https://pubs.acs.org/10.1021/acs.macromol.0c02610

Notes

The authors declare no competing financial interest.

ACKNOWLEDGMENTS

The authors are grateful to the National Science Foundation for the financial support under Grant DMR-2049518 and 1535412.

REFERENCES

(1) Gao, H.; Matyjaszewski, K. Synthesis of molecular brushes by "grafting onto" method: Combination of ATRP and click reactions. *J. Am. Chem. Soc.* **2007**, *129*, 6633−6639.

(2) Hadjichristidis, N.; Xenidou, M.; Iatrou, H.; Pitsikalis, M.; Poulos, Y.; Avgeropoulos, A.; Sioula, S.; Paraskeva, S.; Velis, G.; Lohse, D. J.; Schulz, D. N.; Fetters, L. J.; Wright, P. J.; Mendelson, R. A.; García-Franco, C. A.; Sun, T.; Ruff, C. J. Well-Defined, Model Long Chain Branched Polyethylene. 1. Synthesis and Characterization. *Macromolecules* **2000**, *33*, 2424−2436.

(3) Sheiko, S. S.; Sumerlin, B. S.; Matyjaszewski, K. Cylindrical Molecular Brushes: Synthesis, Characterization, and Properties. *Prog. Polym. Sci.* **2008**, *33*, 759−785.

(4) Rzayev, J. Molecular Bottlebrushes: New Opportunities in Nanomaterials Fabrication. *ACS Macro Lett.* **2012**, *1*, 1146−1149.

(5) Xie, G.; Martinez, M. R.; Olszewski, M.; Sheiko, S. S.; Matyjaszewski, K. Molecular bottlebrushes as novel materials. *Biomacromolecules* **2019**, *20*, 27−54.

(6) Lin, T.-P.; Chang, A. B.; Chen, H.-Y.; Liberman-Martin, A. L.; Bates, C. M.; Voegtle, M. J.; Bauer, C. A.; Grubbs, R. H. Control of grafting density and distribution in graft polymers by living ring-opening metathesis copolymerization. *J. Am. Chem. Soc.* **2017**, *139*, 3896−3903.

(7) Fetters, L. J.; Lohse, D. J.; García-Franco, C. A.; Brant, P.; Richter, D. Prediction of Melt State Poly(α-olefin) Rheological Properties: The Unsuspected Role of the Average Molecular Weight per Backbone Bond. *Macromolecules* **2002**, *35*, 10096−10101.

(8) Haugan, I. N.; Maher, M. J.; Chang, A. B.; Lin, T.-P.; Grubbs, R. H.; Hillmyer, M. A.; Bates, F. S. Consequences of Grafting Density on the Linear Viscoelastic Behavior of Graft Polymers. *ACS Macro Lett.* **2018**, *7*, 525−530.

(9) Dalsin, S. J.; Hillmyer, M. A.; Bates, F. S. Linear Rheology of Polyolefin-Based Bottlebrush Polymers. *Macromolecules* **2015**, *48*, 4680−4691.

(10) Hu, M.; Xia, Y.; McKenna, G. B.; Kornfield, J. A.; Grubbs, R. H. Linear Rheological Response of a Series of Densely Branched Brush Polymers. *Macromolecules* **2011**, *44*, 6935−6943.
(11) Liang, H.; Morgan, B. J.; Xie, G.; Martinez, M. R.; Zhulina, E. B.; Matyjaszewski, K.; Sheiko, S. S.; Dobrynin, A. V. Universality of the Entanglement Plateau Modulus of Comb and Bottlebrush Polymer Melts. *Macromolecules* **2018**, *51*, 10028−10039.
(12) López-Barrón, C. R.; Brant, P.; Eberle, A. P. R.; Crowther, D. J. Linear rheology and structure of molecular bottlebrushes with short side chains. *J. Rheol.* **2015**, *59*, 865−883.
(13) Liang, H.; Grest, G. S.; Dobrynin, A. V. Brush-like Polymers and Entanglements: From Linear Chains to Filaments. *ACS Macro Lett.* **2019**, *8*, 1328−1333.
(14) Daniel, W. F. M.; Burdyńska, J.; Vatankhah-Varnoosfaderani, M.; Matyjaszewski, K.; Paturej, J.; Rubinstein, M.; Dobrynin, A. V.; Sheiko, S. S. Solvent-free, supersoft and superelastic bottlebrush melts and networks. *Nat. Mater.* **2016**, *15*, 183−189.
(15) Abbasi, M.; Faust, L.; Riazi, K.; Wilhelm, M. Linear and Extensional Rheology of Model Branched Polystyrenes: From Loosely Grafted Combs to Bottlebrushes. *Macromolecules* **2017**, *50*, 5964−5977.
(16) Ahmad, N. M.; Lovell, P. A.; Underwood, S. M. Viscoelastic Properties of Branched Polyacrylate Melts. *Polym. Int.* **2001**, *50*, 625−634.
(17) Pakula, T.; Zhang, Y.; Matyjaszewski, K.; Lee, H.-i.; Boerner, H.; Qin, S.; Berry, G. C. Molecular Brushes as Super-Soft Elastomers. *Polymer* **2006**, *47*, 7198−7206.
(18) Cai, L.-H.; Kodger, T. E.; Guerra, R. E.; Pegoraro, A. F.; Rubinstein, M.; Weitz, D. A. Soft Poly(dimethylsiloxane) Elastomers from Architecture-Driven Entanglement Free Design. *Adv. Mater.* **2015**, *27*, 5132−5140.
(19) Vatankhah-Varnosfaderani, M.; Daniel, W. F. M.; Everhart, M. H.; Pandya, A. A.; Liang, H.; Matyjaszewski, K.; Dobrynin, A. V.; Sheiko, S. S. Mimicking biological stress-strain behaviour with synthetic elastomers. *Nature* **2017**, *549*, 497−501.
(20) Liang, H.; Wang, Z.; Dobrynin, A. V. Scattering from Melts of Combs and Bottlebrushes: Molecular Dynamics Simulations and Theoretical Study. *Macromolecules* **2019**, *52*, 5555−5562.
(21) Cao, Z.; Carrillo, J.-M. Y.; Sheiko, S. S.; Dobrynin, A. V. Computer Simulations of Bottle Brushes: From Melts to Soft Networks. *Macromolecules* **2015**, *48*, 5006−5015.
(22) Liang, H.; Vatankhah-Varnoosfaderani, M.; Sheiko, S. S.; Dobrynin, A. V. Computationally driven design of soft materials with tissue-like mechanical properties. In *Gels and Other Soft Amorphous Solids*, Horkay, F.; Douglas, J. F.; Del Gado, E., Eds.; American Chemical Society: Washington, DC, 2019; pp 33−50.
(23) Liang, H.; Sheiko, S. S.; Dobrynin, A. V. Supersoft and Hyperelastic Polymer Networks with Brushlike Strands. *Macromolecules* **2018**, *51*, 638−645.
(24) Liang, H.; Cao, Z.; Wang, Z.; Sheiko, S. S.; Dobrynin, A. V. Combs and Bottlebrushes in a Melt. *Macromolecules* **2017**, *50*, 3430−3437.
(25) Liang, H.; Wang, Z.; Sheiko, S. S.; Dobrynin, A. V. Comb and Bottlebrush Graft Copolymers in a Melt. *Macromolecules* **2019**, *52*, 3942−3950.
(26) Dalsin, S. J.; Rions-Maehren, T. G.; Beam, M. D.; Bates, F. S.; Hillmyer, M. A.; Matsen, M. W. Bottlebrush Block Polymers: Quantitative Theory and Experiments. *ACS Nano* **2015**, *9*, 12233−12245.
(27) Verduzco, R.; Li, X.; Pesek, S. L.; Stein, G. E. Structure, Function, Self-Assembly, and Applications of Bottlebrush Copolymers. *Chem. Soc. Rev.* **2015**, *44*, 2405−2420.
(28) Spencer, R. K. W.; Matsen, M. W. Field-theoretic simulations of bottlebrush copolymers. *J. Chem. Phys.* **2018**, *149*, 184901.
(29) Zhang, J.; Schneiderman, D. K.; Li, T.; Hillmyer, M. A.; Bates, F. S. Design of Graft Block Polymer Thermoplastics. *Macromolecules* **2016**, *49*, 9108−9118.
(30) Vatankhah-Varnosfaderani, M.; Keith, A. N.; Cong, Y.; Liang, H.; Rosenthal, M.; Sztucki, M.; Clair, C.; Magonov, S.; Ivanov, D. A.; Dobrynin, A. V.; Sheiko, S. S. Chameleon-Like Elastomers with Molecularly Encoded Strain-Adaptive Stiffening and Coloration. *Science* **2018**, *359*, 1509−1513.
(31) Sheiko, S. S.; Dobrynin, A. V. Architectural code for rubber elasticity: From supersoft to superfirm materials. *Macromolecules* **2019**, *52*, 7531−7546.
(32) Kremer, K.; Grest, G. S. Dynamics of entangled linear polymer melts: A molecular dynamics study. *J. Chem. Phys.* **1990**, *92*, 5057−5086.
(33) Carrillo, J.-M. Y.; Dobrynin, A. V. Polyelectrolytes in Salt Solutions: Molecular Dynamics Simulations. *Macromolecules* **2011**, *44*, 5798−5816.
(34) De Gennes, P. G. Theory of Long-range Correlations in Polymer Melts. *Faraday Discuss. Chem. Soc.* **1979**, *68*, 96−103.
(35) de Gennes, P. G. *Scaling Concepts in Polymer Physics*; Cornell University Press, 1979.
(36) Yerukhimovich, I. Y. Effect of Chemical Structure of Two-Component Melts of Heteropolymers on the Formation of Domain Structure. *Polym. Sci.* **1982**, *24*, 2232−2241.
(37) Yerukhimovich, I. Y. Fluctuations and the Formation of Domain Structure in Heteropolymers. *Polym. Sci.* **1982**, *24*, 1942−1949.
(38) De Gennes, P. G. Theory of X-ray Scattering by Liquid Macromolecules with Heavy Atom Labels. *J. Phys.* **1970**, *31*, 235−238.
(39) Leibler, L.; Benoit, H. Theory of Correlations in Partly Labelled Homopolymer Melts. *Polymer* **1981**, *22*, 195−201.
(40) Leibler, L. Theory of Microphase Separation in Block Copolymers. *Macromolecules* **1980**, *13*, 1602−1617.
(41) Dobrynin, A. V.; Erukhimovich, I. Y. Computer-aided comparative investigation of architecture influence on block copolymer phase diagrams. *Macromolecules* **1993**, *26*, 276−281.
(42) Debye, P. Molecular-weight Determination by Light Scattering. *J. Phys. Colloid Chem.* **1947**, *51*, 18−32.
(43) López-Barrón, C. R.; Tsou, A. H.; Younker, J. M.; Norman, A. I.; Schaefer, J. J.; Hagadorn, J. R.; Throckmorton, J. A. Microstructure of Crystallizable α-Olefin Molecular Bottlebrushes: Isotactic and Atactic Poly(1-octadecene). *Macromolecules* **2018**, *51*, 872−883.
(44) Sarapas, J. M.; Martin, T. B.; Chremos, A.; Douglas, J. F.; Beers, K. L. Bottlebrush polymers in the melt and polyelectrolytes in solution share common structural features. *Proc. Natl. Acad. Sci. U.S.A.* **2020**, *117*, 5168−5175.
(45) López-Barrón, C. R.; Hagadorn, J. R.; Mattler, S. J.; Throckmorton, J. A. Syndiotactic α-Olefin Molecular Bottlebrushes: Crystallization, Melting, and Hierarchical Microstructure. *Macromolecules* **2020**, *53*, 3778−3788.
(46) Carrillo, J.-M. Y.; Dobrynin, A. V. Polyelectrolytes in Salt Solutions: Molecular Dynamics Simulations. *Macromolecules* **2011**, *44*, 5798−5816.
(47) Keith, A. N.; Clair, C.; Lallam, A.; Bersenev, E. A.; Ivanov, D. A.; Tian, Y.; Dobrynin, A. V.; Sheiko, S. S. Independently Tuning Elastomer Softness and Firmness by Incorporating Side Chain Mixtures into Bottlebrush Network Strands. *Macromolecules* **2020**, *53*, 9306−9312.
(48) Frenkel, D.; Smit, B. *Understanding Molecular Simulations*; Academic Press: New York, 2002.
(49) Plimpton, S. Fast parallel algorithms for short-range molecular dynamics. *J. Comput. Phys.* **1995**, *117*, 1−19.

https://dx.doi.org/10.1021/acs.macromol.0c02610
Macromolecules 2021, 54, 1818−1828